One hundred years of Arctic surface temperature variation due to anthropogenic influence

John C. Fyfe[1], Knut von Salzen[1], Nathan P. Gillett[1], Vivek K. Arora[1], Gregory M. Flato[1]
& Joseph R. McConnell[2]

[1]Canadian Centre for Climate Modelling and Analysis, Environment Canada, Victoria BC, V8W 3R4, Canada, [2]Division of
Hydrologic Sciences, Desert Research Institute, Reno NV, 89512, USA.

Observations show that Arctic-average surface temperature increased from 1900 to 1940, decreased from
1940 to 1970, and increased from 1970 to present. Here, using new observational data and improved climate
models employing observed natural and anthropogenic forcings, we demonstrate that contributions from
greenhouse gas and aerosol emissions, along with explosive volcanic eruptions, explain most of this observed
variation in Arctic surface temperature since 1900. In addition, climate model simulations without natural
and anthropogenic forcings indicate very low probabilities that the observed trends in each of these periods
were due to internal climate variability alone. Arctic climate change has important environmental and
economic impacts and these results improve our understanding of past Arctic climate change and our
confidence in future projections.

P revious studies generally suggest that while the long-term Arctic warming[1–3] is attributable to increasing
greenhouse gas emissions[4–7] the observed multi-decadal variation is primarily associated with internal
climate variability[4,5,8–10]. This observed multi-decadal variation was not captured by previous generation
climate models[4–7]. Early-20th-century warming is also seen in global-average surface temperature which previous
single-model simulations indicate could be explained by some combination of human-induced radiative forcing
and an unusually large realization of multi-decadal variability[11].

Here, we compare Arctic-average (60°N–90°N) annual-average surface temperature from 1900 to 2005 from
the HadCRUT4[12] observational dataset to results from multiple climate models sampled only at locations where
corresponding observations exist. Suitable climate simulations with individual forcings extending past 2005 are
available from only a few models; hence our period of analysis ends in 2005. Multi-model simulations were
obtained from the Coupled Model Intercomparison Project Phase 5 (CMIP5) archive. Three sets of simulations
were available from 18 models. The first set of simulations (ALL) is forced by historical anthropogenic increases in
greenhouses gases, changes in aerosol and aerosol precursor emissions, anthropogenic ozone changes, changes in
land cover and natural forcing. The second set (GHG) is forced by historical increases in anthropogenic green-
house gases, including anthropogenic ozone forcing in five models. The third set (NAT) is forced only by the
historical natural forcing representing solar variability and volcanic aerosol emissions. We estimate the response
to anthropogenic forcings other than greenhouse gases (OTH) by subtracting the simulated temperature anom-
alies in the GHG and NAT simulations from the temperature anomalies in the ALL simulations, based on the
assumption of linearly additive responses to the external forcings.

We also employ additional simulations available from one of the CMIP5 models (CanESM2); these additional
simulations allow us to separate the responses to changes in aerosols (combined sulphate aerosol, organic carbon
and black carbon; AER), black carbon aerosol (BC), land use (LU), solar irradiance (SL), ozone (combined
tropospheric and stratospheric ozone; OZ), stratospheric ozone (SOZ) and methane (CH4). All these responses
were obtained directly (i.e., calculated from simulations in which only one particular forcing is applied), except for
the black carbon and methane responses which were estimated from the difference between the ALL forcing
simulations as above and a corresponding ALL simulation with black carbon aerosol or methane concentrations
fixed at 1850 values.

The CMIP5 models used in this study are HadGEM2-ES (4,N,Y,B), IPSL-CM5A-LR (3,N,Y,B), MIROC-ESM
(3,Y,Y,B), CanESM2 (5,N,Y,B), CSIRO-Mk3-6-0 (5,N,Y,B), MIROC-ESM-CHEM (1,Y,Y,B), NorESM1-M

(1,Y,Y), CNRM-CM5 (6,N,Y), GFDL-CM3 (3,Y,Y), CESM1-CAM5-1-FV2 (2,N,Y), CCSM4 (3,N,N), FGOALS-g2 (1,N,Y), GISS-E2-R (5,N,Y,W), GISS-E2-H (5,N,Y,W), GFDL-ESM2M (1,N,N,W), bcc-csm1-1 (1,N,N,W), MRI-CGCM3 (1,Y,Y,W) and BNU-ESM (1,N,N,W). Indicated in parentheses are the number of simulations, whether time-varying ozone is included in the GHG simulations (Y for yes and N for no), whether the indirect aerosol effect is included (i.e. if Y then the first, and in some cases, second indirect effect is included), and whether the model is a member of the BEST6 (B) or WRST6 (W) ensemble as defined below. The additional sets of CanESM2 simulations each contain five simulations.

Results

Observed interannual to multidecadal variability (i.e. with periods from 2 to 50 years) in Arctic-average surface temperature[12,13] is generally within the 5–95% range found in the ALL simulations with natural and anthropogenic forcings (Figure 1a). The evidence, therefore, indicates that the current generation of climate models reproduces the observed level of interannual to multidecadal variability in Arctic surface temperature. Further, at periods of around 50 years, the variability in the ALL simulations is more than twice that in the control simulations (CON) run without natural and anthropogenic forcings (Figure 1b). Here the control power spectral densities are computed using 92 available 106-year long independent segments
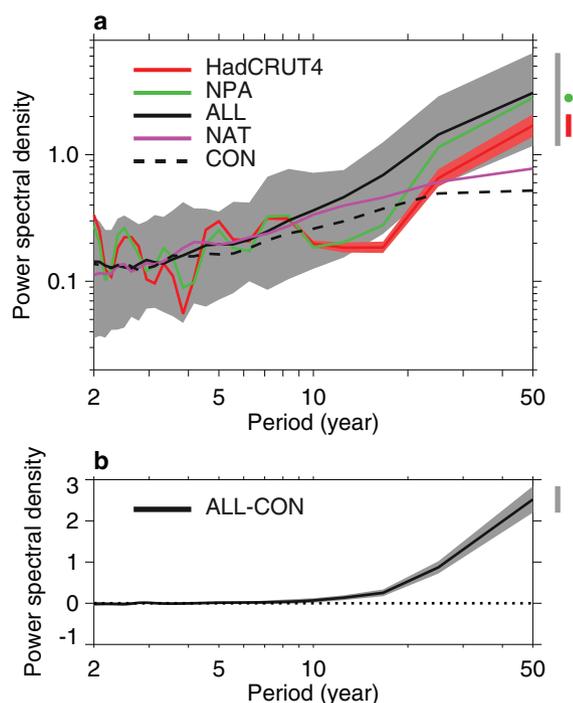
(i.e. corresponding to the 106-year record from 1900–2005) from 17 of the above climate models with available control simulations (CESM1-CAM5-1-FV2 does not have an available control simulation), and where simulated temperatures are used only where corresponding observations exist.

Figure 2 (top panel) shows observed early-20th-century warming, middle-20th-century cooling and late-20th-century warming. To quantify this behaviour, trends were estimated for the 1900–1939, 1939–1970 and 1970–2005 periods. These trends were obtained from piecewise linear approximations over the period from 1900–2005; with the separation years of 1939 and 1970 having been found to be optimal (see Methods). Figure 2 (top panel) also compares the observed Arctic-average annual-average surface temperature anomalies with those averaged over the six sets of simulations whose piecewise linear approximations in their ALL simulations are closest, in the least squares sense, to the observed piecewise linear approximation (BEST6; see Methods). It should be noted that while the observed variability is similar to variability simulated by the individual models it is larger than the variability in the BEST6 ensemble average owing to the smoothing effect of ensemble averaging. The BEST6 ensemble reproduces the observed multi-decadal variation in Arctic-average surface temperature, with early-20th-century warming, middle-20th-century cooling and late-20th-century warming. In quantitative terms, the linear correlation between the observed and the BEST6-average time series of Arctic surface temperature is 0.65. Here we note that the BEST6 Arctic surface temperature evolution appears to combine impacts from GHG, NAT and OTH forcings (Figure 2, bottom panels).
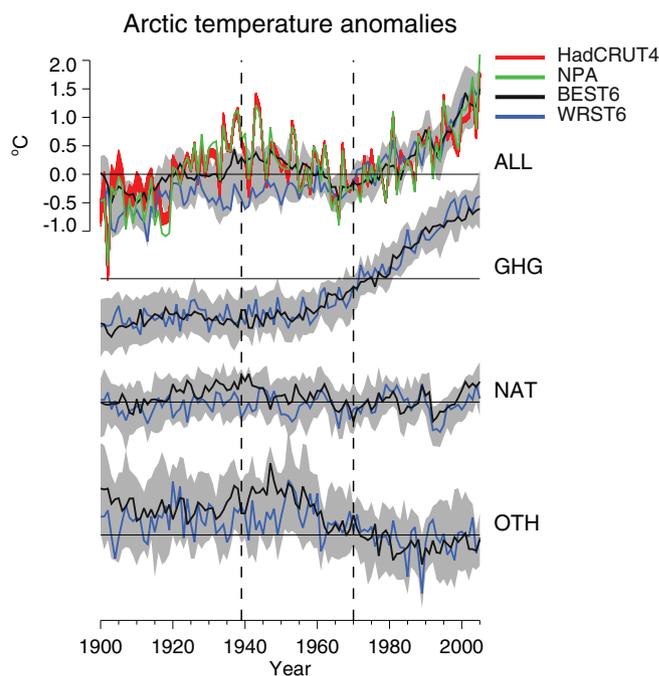

Figure 1 | Power spectral densities of Arctic surface temperature.
(a). Dark red curve is the average over 100 realizations of the near-global HadCRUT4 observations[12], green curve is for North Polar Area (NPA) observations[13], black curve is the average over 51 realizations from 18 CMIP5 models with natural and anthropogenic forcings (ALL), pink curve is the average over 51 realizations from 18 CMIP5 models without anthropogenic forcing (NAT), and the dashed curve is the average over 92 independent realizations from 17 CMIP5 models without natural or anthropogenic forcings (CON). Red shading is the 5–95% range of HadCRUT4 spectra. Grey shading is the 5–95% range of ALL spectra. (b). Black curve is the difference between the ALL-average and CON-average power spectral densities with the 95% confidence interval indicated with grey shading. Spectra are for Arctic-average annual-average surface temperature for the period from 1900–2005, and a Tukey-Hanning window function was used with a width of 25 years.

Figure 2 | Anomalies of Arctic surface temperature. Model simulations are with anthropogenic plus natural (ALL) forcing, greenhouse gas (and ozone forcing in five models; GHG) forcing, natural (combined solar and volcanic; NAT) forcing and other anthropogenic (OTH) forcing. Red curves show 100 realizations of near-global HadCRUT4 observations[12] and the green curve shows North Polar Area (NPA) observations[13]. Black (blue) curves are ensemble-averages over the six CMIP5 simulations with the best (worst) agreement between simulated and observed piecewise linear approximations. Grey shading is ± one standard deviation over the full ensemble of 18 CMIP5 models. Anomalies are relative to the 1961 to 1990 climatology.

The six sets of simulations whose piecewise linear approximations are furthest from the observed piecewise linear approximation (WRST6; see Methods) do not capture the observed multi-decadal variation in Arctic surface temperature, particularly the middle-20th-century cooling. Here the linear correlation between the observed and the WRST6-average time series of Arctic-average surface temperature is 0.48. All of the BEST6 models include some representation of the indirect aerosol effect while half of the WRST6 models do not. This suggests that this effect may be important to capturing the observed multi-decadal variation in Arctic-average surface temperature.

Figure 3 shows observed and simulated trends in Arctic-average surface temperature over the early, middle and late periods of the 1900–2005 temperature record (individual observed and model trends are shown in Supplementary Tables S1–S3 online). In the early-20th-century warming period (1900–1939) the observed trend is consistent (it is within the 95% confidence interval) with the trends in the BEST6 ensemble, with the latter clearly due to NAT warming, and to a lesser extent to OTH warming. Some of the observed warming during this period may also be associated with part of the rapid rise in black carbon aerosol emissions in the late-19th-century and early-20th-century[14], however such a warming impact is not seen in CanESM2 BC simulations. CanESM2 includes representations of the direct and semi-direct effects of black carbon aerosol on climate from scattering and absorption of radiation in the atmosphere. However, the effects of black carbon aerosol on snow and ice albedos, internal mixing of black carbon aerosol with other aerosols, and indirect effects are not included, and emissions may be underestimated. This leads to a positive radiative forcing in CanESM2, and in many other models, that is likely too low compared to observation-based estimates[15]. Finally, while the early-20th-century warming in the BEST6 ensemble is consistent with the observed warming, the mean is about 40% less than observed. The WRST6 ensemble does not show a significant average trend in the early-century period, nor does it show a significant GHG, NAT or OTH response.

In the middle-20th-century cooling period (1939–1970) the observed trend is also consistent with the BEST6 ensemble, although the BEST6-average cooling is about 30% less than observed. In the BEST6 ensemble, significant cooling impacts from NAT and OTH forcing changes overwhelm a significant GHG warming impact. CanESM2, a member of the BEST6 ensemble, captures the middle-20th-century cooling (see Supplementary Table S2 online) and Figure 3 suggests that aerosol (AER) changes are mainly responsible for the middle-20th-century cooling in CanESM2. An anthropogenic aerosol contribution to middle-20th-century cooling was previously inferred using GHG simulations from earlier generation climate models, none of which simulated middle-20th-century cooling, together with an empirical fit to global temperatures and hemispheric temperature gradient[7]. However, our results are the first direct confirmation of this impact. The WRST6 ensemble does not show a significant middle-20th-century cooling trend, nor does it capture any significant NAT or OTH cooling impacts.

In the late-20th-century warming period (1970–2005) the observed trend is consistent with the BEST6 ensemble with the BEST6 trends dominated by GHG warming, as is also true of the WRST6 ensemble. In contrast to an earlier study[7] using past generation climate models together with an empirical fit to global temperatures we find no evidence in the CMIP5 multi-model ensemble that changes in aerosols since the 1970s (here part of OTH) have contributed to recent Arctic warming.

As for trends over the full period from 1900–2005 (see Supplementary Figure S1 online) we note that observed Arctic warming during this period is highly consistent with the BEST6 ensemble, reflecting GHG warming partially offset by OTH cooling in the BEST6 ensemble, and more specifically AER cooling in the CanESM2 ensemble. We also note that long-term changes in anthropogenic ozone has a significant warming impact in the CanESM2 ensemble. The anthropogenic ozone warming impact of about 0.03°C per decade simulated in CanESM2 is consistent with that in the NASA Goddard Institute for Space Studies (GISS) chemistry
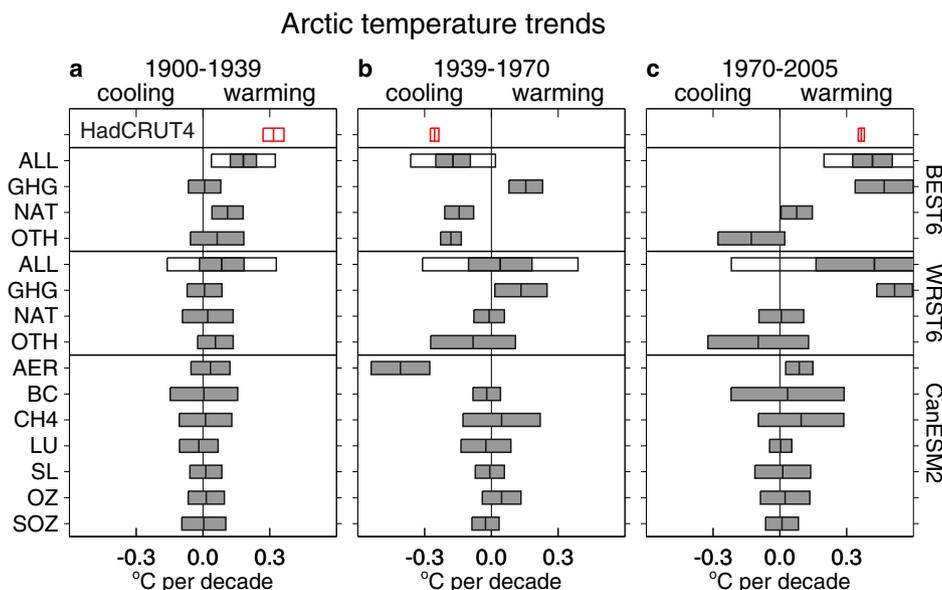
Arctic temperature trends

Figure 3 | Trends in Arctic surface temperature. (a). 1900–1939. (b). 1939–1970. (c). 1970–2005 for HadCRUT4 (first section), BEST6 (second section) WRST6 (third section) and CanESM2 (last section). Red boxes show the 2.5–97.5% ranges of observed trend values with the ranges computed using a two-tailed student t-distribution with $n = 100$. These ranges reflect observational uncertainty. Unshaded black boxes in the BEST6 and WRST6 sections show the 2.5–97.5% ranges of simulated trends, with the ranges computed using a two-tailed student t-distribution with $n = 6$ (trends being first averaged over each model set of realizations). An observed trend lying within this range indicates consistency between it and the model-average trend at the 95% confidence level. The shaded black boxes are the 95% confidence intervals of model-average trends in the case of the BEST6 and WRST6 ensembles ($n = 6$), and realization-average trends in the case of the CanESM2 ensemble ($n = 5$). Such intervals that do not include zero indicate that the model-average or realization-average trend, as the case may be, is significantly different from zero at the 95% confidence level.

model[16]. We find that methane caused a warming impact of about 0.04°C per decade; while we find no significant impact of changes in black carbon aerosol, land use, solar or stratospheric ozone on Arctic-average surface temperature.

Our results suggest that reproducing the observed multi-decadal variation in Arctic surface temperature requires a strong middle-20th-century cooling impact from anthropogenic aerosols. Figure 4a compares the observed sulphate aerosol (SO₄) deposition over Greenland derived from ice core records[17] with that simulated by three of the BEST6 models (CanESM2, CSIRO-Mk3-6-0 and MIROC-ESM) and three of the WRST6 models (MRI-CGCM3, GISS-E2-R and BNU-ESM), these being the models with available wet and dry SO₄ deposition rates. These BEST6 models and CanESM2 in particular, reproduce the change in SO₄ deposition whereas the WSRT6 models either grossly underestimate the change (MRI-CGCM3 and BNU-ESM) or overestimate the change (GISS-E2-R), this despite the fact that the same SO₂ emissions should have been prescribed in all the models. The fact that the GISS-E2-R model shows too much deposition suggests SO₄ removal processes in this model that are too efficient, leaving, as we shall see, too little SO₄ in the atmosphere to produce middle-20th-century cooling. Disparities such as these between climate model simulations are the consequence of differing treatments of sulphate aerosol and cloud physical and chemical processing[18].

Figure 4b compares the observed climatological monthly variation (1980–2005) in the surface concentration of sulphate aerosol for Alert (83°N, 63°W)[19] with that simulated by one of the BEST6 models (CanESM2), two of the WRST6 models (GISS-E2-R and GFDL-ESM2M) and one of the in-between models (GFDL-CM3), these

being the models with available SO₄ surface concentrations at this time. CanESM2 closely reproduces the monthly variation in SO₄ surface concentration whereas the WRST6 models do not. Figure 4c similarly shows that the WRST6 models have much less total SO₄ burden in the atmosphere compared to CanESM2; noting that observed values of total SO₄ burden are unavailable. As inferred earlier the GISS-E2-R model underestimates the amount of the SO₄ in the atmosphere during this period. These results suggest that the BEST6 models mostly reproduce the observed multi-decadal variation of Arctic surface temperature because they reasonably accurately deposit, retain and respond to sulphate aerosols transported into the Arctic from their Northern midlatitude source regions.

Role of natural climate variability. We have shown that most but not all of the multi-decadal variation in Arctic surface temperature is due to the responses to external forcings. We now consider the role of natural climate variability. Using an established multivariate statistical technique[20,21] (see Methods) we estimate the natural signals in Arctic-average monthly-average surface temperature associated with dynamically-induced atmospheric variability, the El Niño-Southern Oscillation (ENSO) and major explosive volcanic eruptions in the HadCRUT4 dataset and in the ALL simulations. The observed signals of dynamically-induced atmospheric variability and explosive volcanic eruptions are significant and together explain 30% of the standard deviation of Arctic-average monthly-average surface temperature (see Supplementary Table S4 online). Importantly, we note a warming impact in the early-20th-century associated with the eruption of Santa Maria in 1902, and a cooling impact in the middle-20th-century associated with the eruption on Agung in 1963
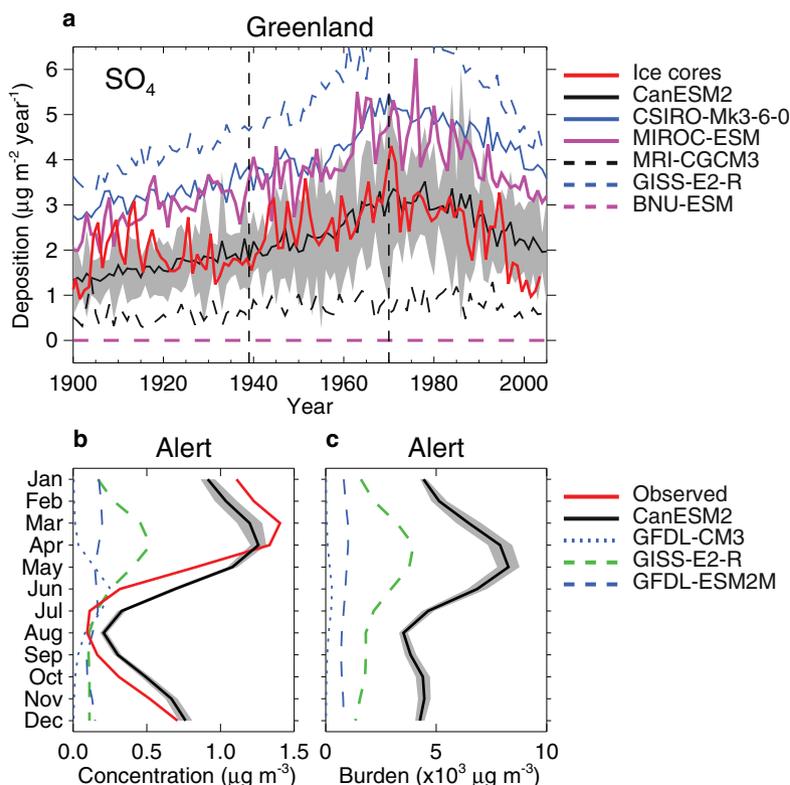

Figure 4 | Sulphate aerosol deposition, concentration and burden in the Arctic. (a). Annual-average deposition over Greenland. The red curve shows observed SO₄ deposition rate averaged over ice core records at the Act2 (66.0°N, 45.2°W), D4 (71.4°N, 43.9°W), Humboldt (78.5°N, 56.8°W), and Summit_2010 (72.6°N, 38.3°W) sites. The other curves are simulated deposition rates averaged over 66.0°N–78.5°N and 56.8°W–38.3°W. (b). Climatological monthly-average SO₄ surface concentration for the 1980–2005 period. The red curve is observed concentration at Alert (82.5°N, 62.3°W). The other curves are simulated concentrations averaged over 80.0°N–85.0°N and 65.0°W–60.0°W. (c). As in (b) but for total SO₄ burden in the atmosphere. The grey shadings are 2.5–97.5% ranges of CanESM2 values. Solid, dashed and dotted curves are BEST6, WRST6 and other simulations, respectively.

(see Supplementary Figure S2 online). The simulated signals of dynamically-induced atmospheric variability and explosive volcanic eruptions are also generally significant and on average explain about 24% of the standard deviation of simulated Arctic-average monthly-average surface temperature (see Supplementary Table S4 online). The simulated volcanic signals contribute, as observed, to the early-period warming and middle-period cooling of Arctic-average surface temperature (see Supplementary Figure S2 online).

Based on earlier results regarding variations in Arctic temperature connected with heat transported from the Atlantic Ocean into Arctic Ocean[9] we explore the connection to the Atlantic Multidecadal Oscillation[22] (AMO). We obtain the AMO signal in Arctic surface temperature by regression of its index[23] (defined here as the average North Atlantic sea surface temperature minus the global average) against Arctic-average monthly-average surface temperature after removing the signals of dynamically-induced atmospheric variability, ENSO and explosive volcanic activity (see Methods). The observed AMO signal (see Supplementary Figure S2 online) is statistically significant and explains about 16% of the standard deviation of Arctic-average monthly-average surface temperature (see Supplementary Table S4 online). Figure 5 shows that the observed AMO signal accounts for about 15%, 30% and 10% of the early-20th-century warming, middle-20th-century cooling and late-20th-century warming in Arctic-average surface temperature, respectively. Two recent studies[24,25] similarly indicate that the AMO contributed to early-20th-century warming, middle-20th-century cooling and late-20th-century warming in global-average surface temperature.

Neither the CMIP5 models, as a group, nor the BEST6 models, as a subset, show a significant signal of the AMO in Arctic-average surface temperature in their ALL simulations (see Supplementary Figure S2 and Table S4 online), hence their AMO signals do not contribute to early-20th-century warming, middle-20th-century cooling or late-20th-century warming (Figure 5). As an aside, it is worth noting that an anthropogenic aerosol influence on the AMO in HadGEM2-ES has been previously reported[26], however this is not seen in other CMIP5 models[27], and is at odds with observations of North Atlantic upper-ocean heat content[28]. Finally, Figure 5 shows that with the observed and simulated AMO signals removed (ALL-AMO) there is an even closer overall agreement between the observed and BEST6 Arctic-average surface temperature trends than found with the AMO signal included. The evidence, therefore, indicates that the observed multi-decadal variation of Arctic-average surface temperature is the consequence of anthropogenic forcing, explosive volcanic eruptions, and AMO influence.

Observed global-average surface temperature similarly shows a multi-decadal variation, albeit with much smaller amplitude than

in the Arctic, which the BEST6 ensemble captures (see Supplementary Figure S3 online). Here we note that the BEST6 models, while optimal in describing observed Arctic-average variation, are as a group no better or no worse than the other members of the CMIP5 ensemble in describing the observed global-average variation. This said, reproducing the observed temporal variations in surface temperature across all regions of the globe, and in the global-average, is a challenge for climate models[7].

Discussion

Observations show that Arctic-average surface temperature increased from 1900 to 1940, decreased from 1940 to 1970, and increased from 1970 to present. Our results show that this multi-decadal variation in Arctic-average surface temperature is better simulated in an ensemble of current climate models that reasonably accurately simulate the transport, deposition and retention of anthropogenic sulphate aerosol into and within the Arctic. Using an ensemble of models run with natural forcings only, as one set of simulations, and anthropogenic-only-forcings, as another set of simulations, we have shown that these multi-decadal variations can be largely explained by local responses to large-scale climate forcings together with a smaller contribution from internal climate variability, notably variability associated with sea surface temperature fluctuations in the North Atlantic. More specifically, we have concluded that the observed Arctic-average surface warming from 1900 to 1939 was likely the combined surface response to rising black carbon aerosol emissions, recovery from the eruption of Santa Maria (1902) at the beginning of the period, and transition of the AMO to its positive phase. We have also argued that observed Arctic-average surface cooling from 1939–1970 was due to anthropogenic sulphate aerosol cooling, the eruption of Agung (1963) towards the end of the period and the transition of the AMO to its negative phase – a combined cooling effect that overwhelmed a significant GHG warming impact during this period. Arctic-average surface warming from 1970–2005 was dominated by GHG warming with a smaller contribution from the transition of the AMO to its positive phase. Our analysis has also identified a number of deficiencies in many current climate models, most notably the incomplete representation of the effects of anthropogenic sulphate aerosols and black carbon aerosols on climate, which together contribute to the inability of some models to reproduce observed Arctic surface temperature trends and to the inter-model spread in trends across all models.

Finally, using this set of current climate models run without natural and anthropogenic forcings it is possible to estimate the probability that the observed variation in Arctic-average surface temperature was due to internal climate variability alone. To
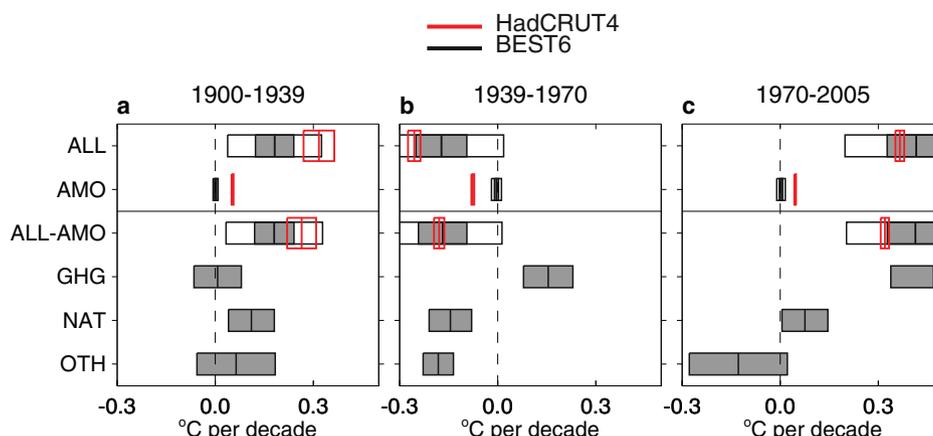

Figure 5 | Atlantic Multidecadal Oscillation signal in Arctic surface temperature trends. (a). 1900–1939. (b). 1939–1970. (c). 1970–2005. As in Figure 3 but also showing trends associated with the signal of the Arctic Multidecadal Oscillation (AMO) in Arctic-average surface temperature (second row) and trends in Arctic-average surface temperature after removing these signals of the AMO (third row). With the signals of the AMO removed there is an even closer agreement between observed and BEST-average Arctic surface temperature evolution.
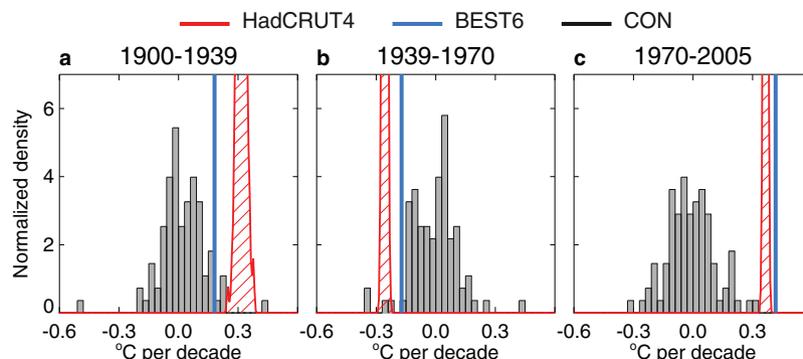
Figure 6 | Arctic surface temperature trends. (a). 1900–1939. (b). 1939–1970. (c). 1970–2005. For the observations, 100 realizations of the HadCRUT4 ensemble are used (red hatching). For the models, 92 realizations from 17 climate models without natural or anthropogenic forcings are used (grey shading). Blue vertical lines show the BEST6-average trends based 21 realizations from 6 climate models with natural and anthropogenic forcings.

accomplish this we have taken all available 106-year long independent segments from 17 of the above climate models with available control (i.e. externally-unforced) simulations. In total this yielded 92 such segments which were each masked with the observational coverage before computing piecewise linear approximations as above. Figure 6 shows that only one such segment, or realization, has early-20th-century warming as large as observed, and that only two realizations have middle-20th-century cooling as large as observed – no realizations have late-20th-century warming as large as observed. The evidence, therefore, suggests that internal climate variability cannot account for the observed trends, and this is supported by statistical tests of the null hypothesis that observed trends are consistent with zero[29]. Differences between observed and control–average trends in the early-20th-century and middle-20th-century periods have p-values equal to 0.01 and 0.02, respectively, and near zero for the late-20th-century period (assuming the models are exchangeable with each other[29]). Here we note that the smaller the p-value is, the stronger the evidence against the null hypothesis. On this basis, we reject the null hypothesis that the observed trends are due to internal climate variability. In contrast, differences between the observed and BEST6–average trends in the early-20th-century, middle-20th-century and late 20th-century-periods have p-values equal to 0.08, 0.17 and 0.30, respectively. Hence, only with simulations that combine natural and anthropogenic (aerosol) forcings can we explain the observed variation in Arctic-average surface temperature from 1900–2005.

Since observations of internal climate variability are unavailable (reliable paleo-observations of Arctic wide surface temperature do not exist) we have used climate model control (i.e. externally-unforced) simulations to estimate this variability. To judge the sensitivity of results to our model-based estimate of internal climate variability we note that doubling the variance of this estimate (i.e. by multiplying the control trends in Figure 6 by the square root of 2) does not affect our conclusion that internal climate variability cannot explain the variation in Arctic-average surface temperature variability from 1900–2005.

Methods

Piecewise linear approximations. We approximate Arctic-average annual-average surface temperature $T(t)$ using piecewise linear functions in three pieces between $t_1 =$ 1900 and $t_4 =$ 2005:

$$F(t) = \begin{cases} T_1 + (T_2 - T_1)(t - t_1)/(t_2 - t_1) & \text{if} \quad t_1 \le t \le t_2 \\ T_2 + (T_3 - T_2)(t - t_2)/(t_3 - t_2) & \text{if} \quad t_2 \le t \le t_3 \\ T_3 + (T_4 - T_3)(t - t_3)/(t_4 - t_3) & \text{if} \quad t_3 \le t \le t_4. \end{cases}$$

For fixed separation points t_2 and t_3, values of T_i are obtained by setting $\partial Q / \partial T_i = 0$ where $Q = \sum_i (T - F)^2$ and solving the resulting system of four linear equations. The separation points $t_2 = 1939$ and $t_3 = 1970$ produce the best such approximation to the observed time series given pieces each with length greater than 10 years, and these

separation points are used in all cases. Trends in each piece are $\beta_i = (T_{i+1} - T_i)/(t_{i+1} - t_i)$ for $i = 1, 2, 3$.

BEST6 and WRST6 ensembles. These ensembles were selected by first computing the sum of square errors between the observed piecewise linear approximation and the piecewise linear approximations of each simulated ALL time series, i.e. for each of 51 simulations from 18 models. The models were then ranked based on the least sum of square errors over the available simulations for each model, e.g. the sum of square errors was computed for each of CanESM2's five simulations and the smallest of these values determined its ranking relative to the other 17 models. Our conclusions were found to be insensitive to reasonable variations in this procedure including removing the AMO signal before ranking.

Natural signals of Arctic surface temperature variability. Indices in Arctic-average monthly-average surface temperature of dynamically-induced variability, ENSO and volcanic variability were estimated as follows[20,21]. *Dynamically-induced indices* were found on a month-by-month basis by regressing sea level pressure anomaly maps onto normalized land-ocean surface temperature difference time series for the Northern Hemisphere. The coefficient time series of these sea level pressure regression patterns define the index of dynamically-induced variability. *ENSO indices* were estimated using a simple ocean mixed layer model using estimates of monthly anomalous flux of sensible and latent heat in the eastern tropical Pacific and optimal estimates of linear damping and effective heat capacity. *Volcanic indices* were estimated from the oceanic mixed layer model as above with observed aerosol optical thickness data and optimal estimates of linear damping and effective heat capacity. *AMO indices* were estimated using monthly sea surface temperature anomalies averaged over the North Atlantic (75°W–7°W, 25°N–60°N) after subtracting anomalies of global-average surface temperature. Natural signals of dynamically-induced variability, ENSO and volcanic variability in Arctic surface temperature were obtained using a multivariate linear regression of their indices, in addition to a term linear in time, upon Arctic-average monthly-average surface temperature assuming a first order autoregressive, AR(1), model for the noise. The natural signal of the AMO in Arctic surface temperature was obtained by regression of the AMO index against Arctic-average monthly-average surface temperature after first removing the signals of dynamically-induced variability, ENSO and volcanic variability as above. As a final step these natural signals of variability were annually averaged.

1. *ACIA, Arctic Climate Impact Assessment.* Cambridge University Press, 1042p (2005).
2. Trenberth, K. E. *et al. Observations: Surface and Atmospheric Climate Change.* In: Climate Change 2007: The Physical Science Basis. Contribution of Working Group I to the Fourth Assessment Report of the Intergovernmental Panel on Climate Change [Solomon, S., Qin, D., Manning, M., Chen, Z., Marquis, M., Averyt, K. B., Tignor, M. & Miller, H. L. (Eds.)]. Cambridge University Press, Cambridge, United Kingdom and New York, NY, USA (2007).
3. Polyakov, I. V. *et al.* Variability and trends of air temperature and pressure in the maritime Arctic. *J. Climate* **16**, 2067–2077 (2003).
4. Johannessen, O. M. *et al.* Arctic climate change: Observed and modelled temperature and sea ice variability. *Tellus A* **56**, 328–341 (2004).
5. Wang, M. *et al.* Intrinsic versus forced variation in Coupled Climate Model simulations over the Arctic during the Twentieth Century. *J. Climate* **20**, 1093–1107 (2007).
6. Gillett, N. P. *et al.* Attribution of polar warming to human influence. *Nat. Geosci.* **1**, 750–754 (2008).
7. Shindell, D. & Faluvegi, G. Climate response to regional radiative forcing during the twentieth century. *Nat. Geosci.* **2**, 294–300 (2009).
8. Wood, K. R. & Overland, J. E. Early 20th century Arctic warming in retrospect. *Int. J. Climatol.* **30**(9), 1269–1279 (2009) DOI: 10.1002/joc.1973.

9. Bengtsson, L., Semenov, V. A. & Johannessen, O. M. The early twentieth-century warming in the Arctic - a possible mechanism. *J. Climate* **17**, 4045–4057 (2004).
10. Moritz, R. E., Bitz, C. M. & Steig, E. J. Dynamics of recent climate change in the Arctic. *Science* **297**, 1497–1502 (2002).
11. Delworth, T. L. & Knutson, T. R. Simulation of early 20th century global warming. *Science* **287**, 2246–2250 (2000).
12. Morice, C. P., Kennedy, J. J., Rayner, N. A. & Jones, P. D. Quantifying uncertainties in global and regional temperature change using an ensemble of observational estimates: The HadCRUT4 data set. *J. Geophys. Res.* **117** (2012) DOI: 10.1029/2011JD017187.
13. Bekryaev, R. V., Polyakov, I. V. & Alexeev, V. A. Role of polar amplification in long-term surface air temperature variations and modern Arctic warming. *J. Climate* **2**, 3888–3906 (2010).
14. McConnell, J. R. *et al.* 20th century industrial black carbon emissions altered Arctic climate forcing. *Science* **317**, 1381–1384 (2007).
15. Bond, T. C. *et al.* Bounding the role of black carbon in the climate system: A scientific assessment. *J. Geophys. Res.* **118**, 5380–5552 (2013).
16. Shindell, D., Faluvegi, G., Lacis, A., Hansen, J., Ruedy, R. & Aguilar, E. Role of tropospheric ozone increases in 20th century climate change. *J. Geophys. Res.* **111** (2006) doi: 10.1029/2005JD006348.
17. McConnell, J. R. New Directions: Historical black carbon and other ice core aerosol records in the Arctic for GCM evaluation. *Atmos. Environ.* **44**, 2665–2666 (2010).
18. Shindell, D. T. *et al.* A multi-model assessment of pollution transport to the Arctic. *Atmos. Chem. Phys.* **8**, 5353–5372 (2008).
19. Sharma, S., Lavoue, D., Cachier, H., Barrie, L. A. & Gong, S. L. Long-term trends of the black carbon concentrations in the Canadian Arctic. *J. Geophys. Res.* **109** (2004) doi: 10.1029/2003JD004331.
20. Thompson, D. W. J., Wallace, J. M., Jones, P. D. & Kennedy, J. J. Identifying signatures of natural climate variability in time series of global mean surface temperature: Methodology and insights. *J. Climate* **22**, 6120 (2009).
21. Fyfe, J. C., Gillett, N. P. & Thompson, D. W. J. Comparing variability and trends in observed and modelled global-mean surface temperature. *Geophys. Res. Lett.* **37** (2010) doi: 10.1029/2010GL044255.
22. Schlesinger, M. E. & Ramankutty. An oscillation in the global climate system of period 65–70 years. *Nature* **367**, 723–726 (1994).
23. van Oldenborgh, G. J., te Raa, L. A., Dijkstra, H. A. & Philip, S. Y. Frequency- or amplitude-dependent effects of the Atlantic meridional overturning on the tropical Pacific Ocean. *Ocean Sci.* **5**, 293–301 (2009).
24. Tung, K. K. & Zhou, J. Using data to attribute episodes of warming and cooling in instrumental records. *P. Natl. Acad. Sci. USA* **110**, 2058–2063 (2013).
25. Zhou, J. & Tung, K. K. Deducing Multidecadal Anthropogenic Global Warming Trends Using Multiple Regression Analysis. *J. Atmos. Sci.* **70**, 3–8 (2013).
26. Booth, B. B., Dunstone, N. J., Halloran, P. H., Andrews, T. & Bellouin, N. Aerosols implicated as a prime driver of twentieth-century North Atlantic climate variability. *Nature* **484**, 228–232 (2012).
27. Chiang, J. C. H., Chang, C. Y. & Wehner, M. F. Long-term trends of the Atlantic Interhemispheric SST gradient in the CMIP5 historical simulations. *J. Climate* (2013) doi: 10.1175/JCLI-D-12-00487.1.
28. Zhang, R. *et al.* Have aerosols caused the observed Atlantic multi-decadal variability? *J. Atmos. Sci.* **70**, 1135–1144 (2013).
29. Fyfe, J. C., Gillett, N. P. & Zwiers, F. W. Overestimated global warming in the past 20 years. *Nat. Clim. Chang.* **3**, 767–769 (2013).

Acknowledgements

Author contributions

Additional information